

Electronic Supplementary Information for

**An *rht*-type metal-organic framework constructed from an unsymmetrical ligand  
exhibiting high hydrogen uptake capability**

**Jian Li,<sup>‡*a*</sup> Pei-Zhou Li,<sup>‡*b*</sup> Qiu-Yan Li,<sup>*a*</sup> Yang Cao,<sup>*a*</sup> Han Lu,<sup>*a*</sup> Hui Wu,<sup>*c*</sup> Fei Li,<sup>*d*</sup> Yanhui Shi,<sup>*a*</sup> Xiao-Jun Wang<sup>\**a*</sup>  
and Yanli Zhao<sup>\**b*</sup>**

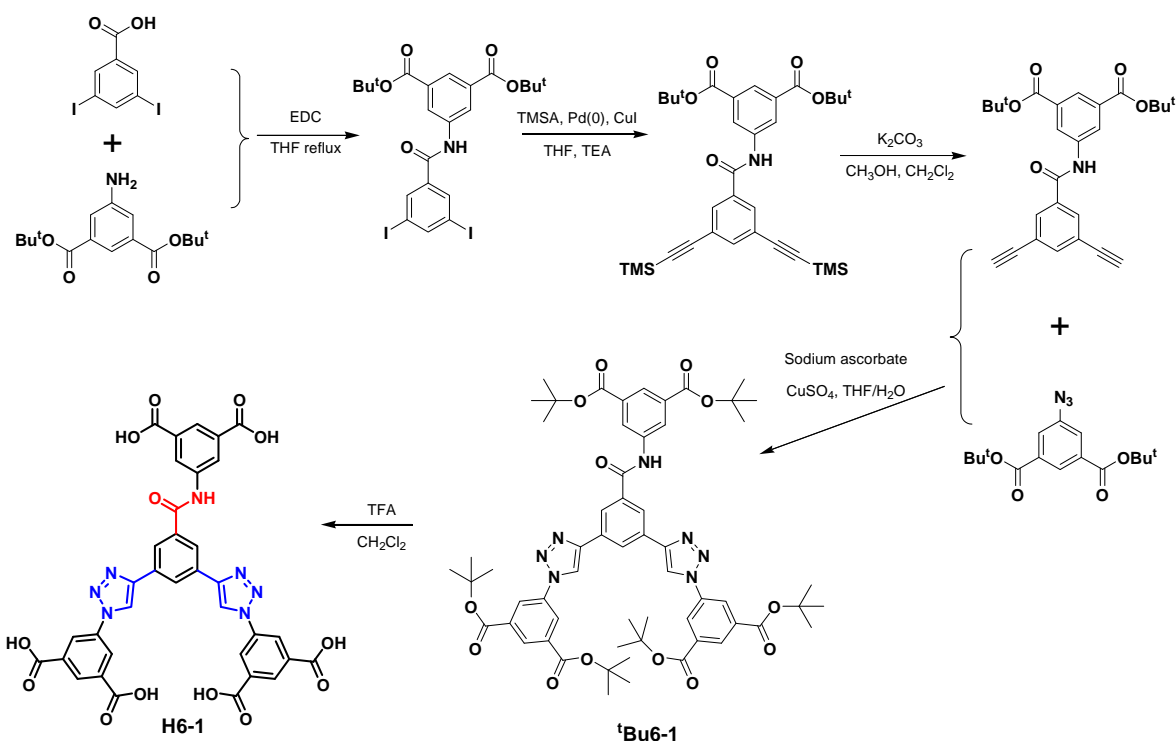
<sup>*a*</sup> School of Chemistry and Chemical Engineering and Jiangsu Key Laboratory of Green Synthetic Chemistry for Functional Materials, Jiangsu Normal University, Xuzhou 221116, P. R. China. E-mail: [xjwang@jsnu.edu.cn](mailto:xjwang@jsnu.edu.cn)

<sup>*b*</sup> Division of Chemistry and Biological Chemistry, School of Physical and Mathematical Sciences, Nanyang Technological University, 637371, Singapore. E-mail: [zhaoyanli@ntu.edu.sg](mailto:zhaoyanli@ntu.edu.sg)

<sup>*c*</sup> Key Laboratory of Biotechnology for Medicinal Plants of Jiangsu Province, Jiangsu Normal University, Xuzhou 221116, P. R. China.

<sup>*d*</sup> Department of Chemistry & Chemical Biology, University of New Mexico, 300 Terrace St. NE, Albuquerque, NM, 87131-0001, USA.

‡ These authors contributed equally to this work.



**Scheme S1.** Synthetic route for ligand **H6-1**. EDC = 1-ethyl-3-(3-dimethylaminopropyl)carbodiimide; THF = tetrahydrofuran; TMSA = trimethylsilylactylene; TEA = triethylamine; TFA = trifluoracetic acid.

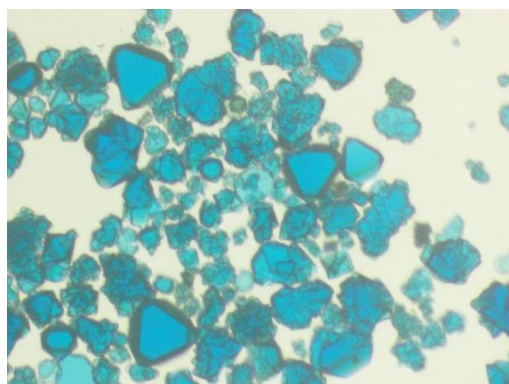


**Fig. S1** The photograph of crystals of as-synthesized **Cu-ABTA**, showing they have good and regular morphologies and shapes.

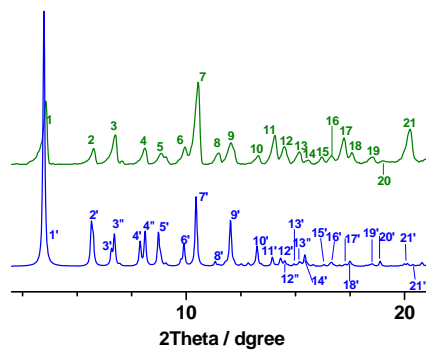


**Fig. S2** The zoomed-in comparison of PXRD patterns ( $2\text{Theta} = 2\text{-}21^\circ$ ) of as-synthesized MOF **Cu-ABAT** (upper) and simulation from MOF **NTU-105** (bottom) single crystal data. Although some of peaks in **NTU-105** ( $3'$  and  $3''$ ;  $4'$  and  $4''$ ;  $12'$  and  $12''$ ;  $13'$  and  $13''$ ;  $21'$  and  $21''$ ) are merged into corresponding one peak in **Cu-ABTA**, mainly due to the different organic ligand in the two MOFs. However, most of the position of main peaks matches very well. This indicates that the overall framework structure of **Cu-ABTA** is the same as that of MOF **NTU-105**.

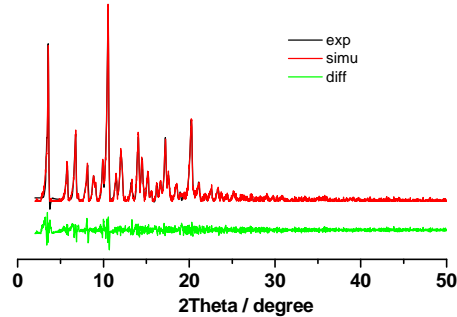


**Fig. S3** Experimental (black), calculated (red), and difference (green below observed and calculated patterns) X-ray powder diffraction profiles for **Cu-ABTA**. All diffraction patterns were indexed using DICVOL9113 to obtain lattice parameters that were subsequently refined in a Pawley fit. A modified Thompson-Cox-Hastings pseudo-Voigt profile function with a simple axial correction was used in TOPAS (Topas V3.0: General Profile and Structure Analysis Software for Powder Diffraction Data Bruker AXS Ltd, 2004). The cell parameters are  $a = 30.03 \text{ \AA}$ ,  $b = 30.03 \text{ \AA}$ ,  $c = 43.11 \text{ \AA}$ ,  $\alpha = 90^\circ$ ,  $\beta = 90^\circ$ ,  $\gamma = 90^\circ$  with a tetragonal space group  $I4/m$ , which are close to those of **NTU-105**. The results of PXRD measurements and simulation indicate that **Cu-ABTA** still possesses the same (3,24)-connected *rht*-framework as our reported MOF **NTU-105**.

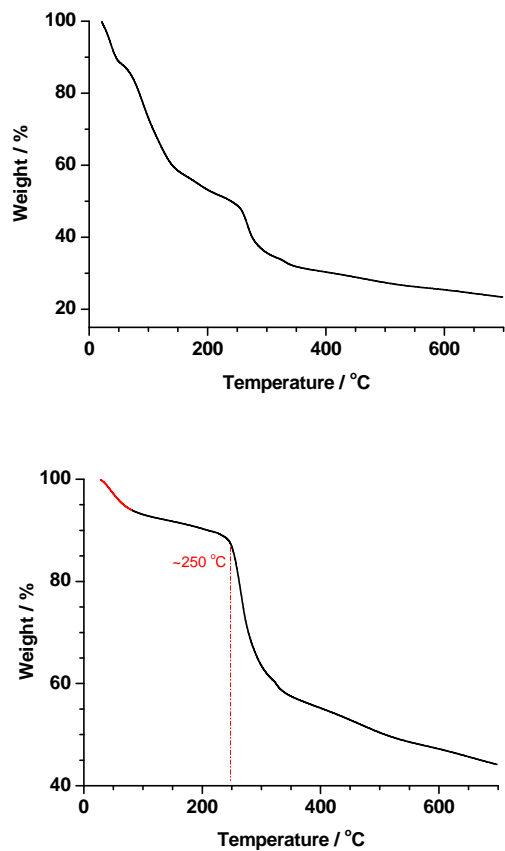


**Fig. S4** TGA plot of as-synthesized (upper) and desolvated (bottom) MOF **Cu-ABTA**. The initial weight loss (red line) of activated sample can be attributed to the readsorbed water during sample weighing. This suggests the framework was stable up to  $\sim 250$   $^{\circ}\text{C}$ , which is similar to **NTU-105**.

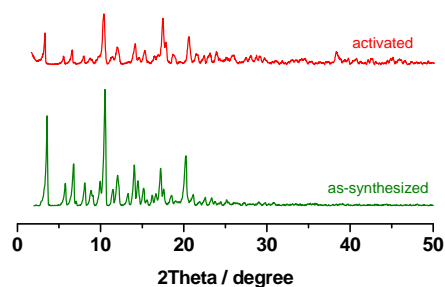


**Fig. S5** XRD pattern of desolvated **Cu-ABTA** (indicating the framework was retained well after activation).

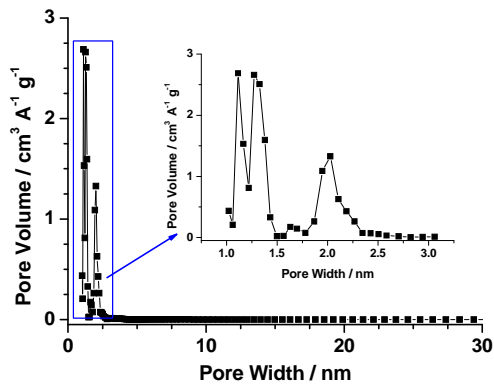


**Fig. S6** Pore-size distribution plot for **Cu-ABTA** as calculated from experimental  $\text{N}_2$  adsorption isotherm using the nonlocal denity functional theory (NLDFT).

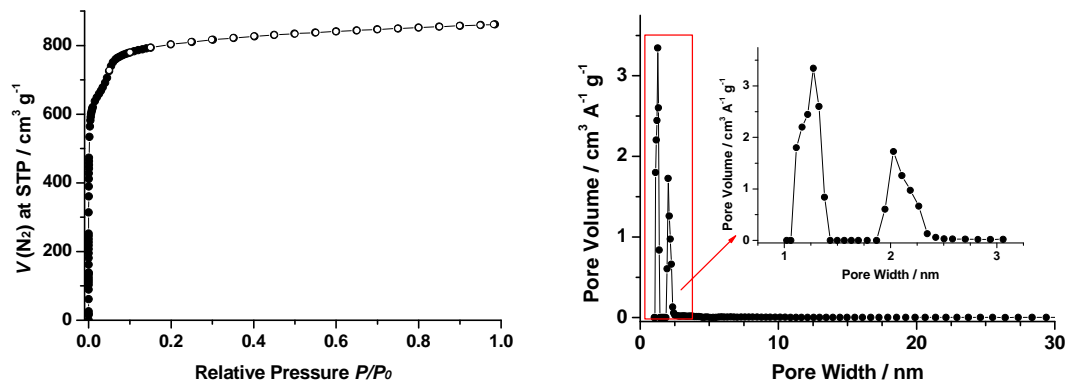


**Fig. S7**  $\text{N}_2$  sorption isotherm (left) at 77 K and pore-size distribution plot (right) for **NTU-105** as calculated from experimental  $\text{N}_2$  adsorption isotherm using the NLDFT.

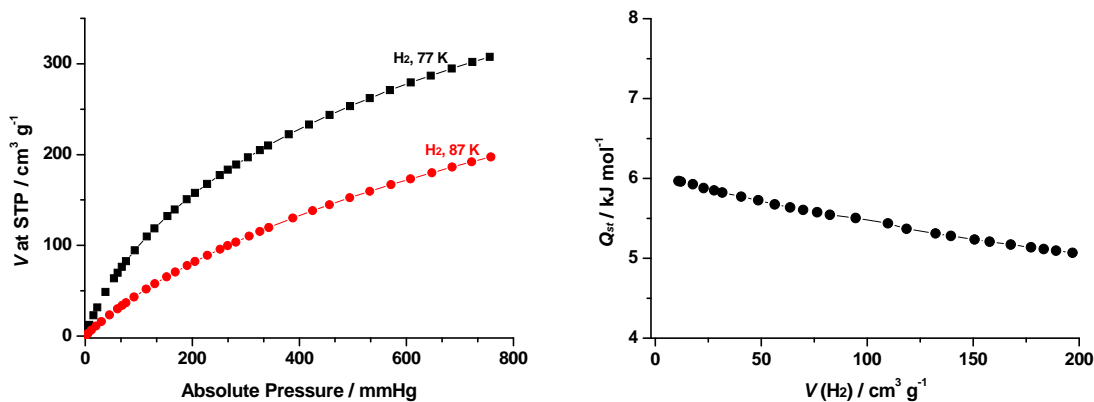


**Fig. S8**  $\text{H}_2$  adsorption isotherms (left) and isosteric heat of  $\text{H}_2$  adsorption (right) for **NTU-105** calculated from the adsorption isotherms at 77 K and 78 K.

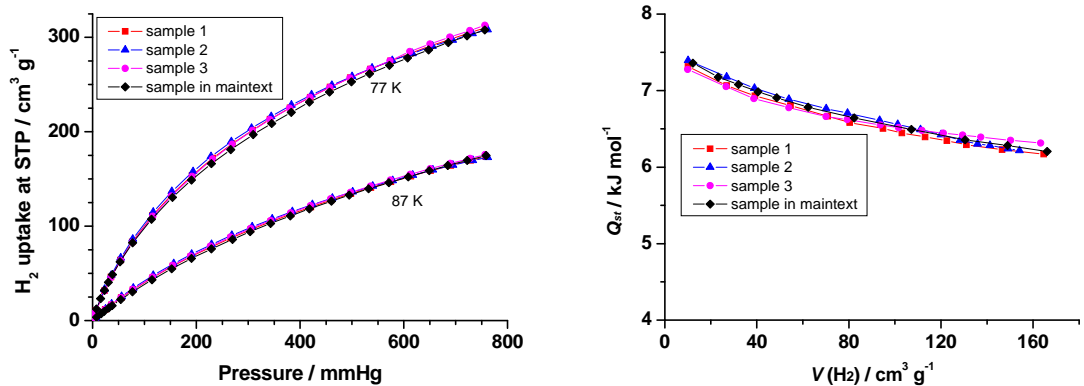


**Fig. S9** Another three hydrogen sorption measurements for MOF **Cu-ABTA** (and corresponding  $Q_{\text{st}}$  calculated from the adsorption isotherms at 77 K and 78 K) by using different samples every time to avoid the accidental error. These indicated the good reproducibility.

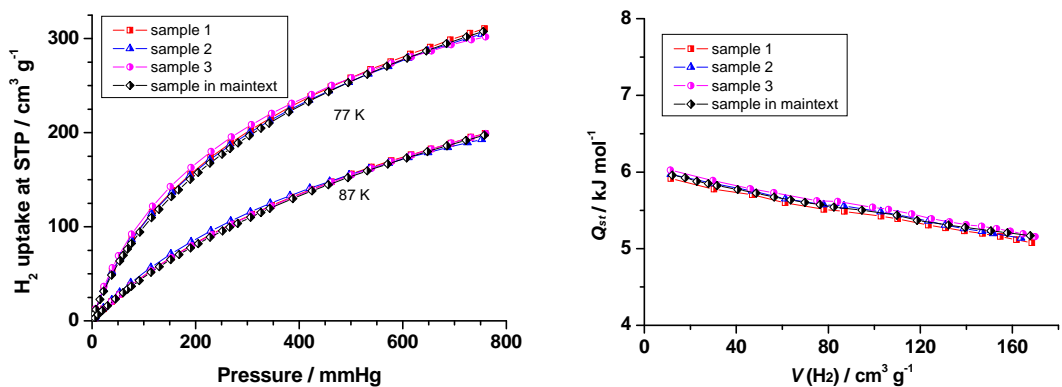


**Fig. S10** Another three hydrogen sorption measurements for MOF **NTU-105** (and corresponding  $Q_{\text{st}}$  calculated from the adsorption isotherms at 77 K and 78 K) by using different samples every time to avoid the accidental error. These indicated the good reproducibility.

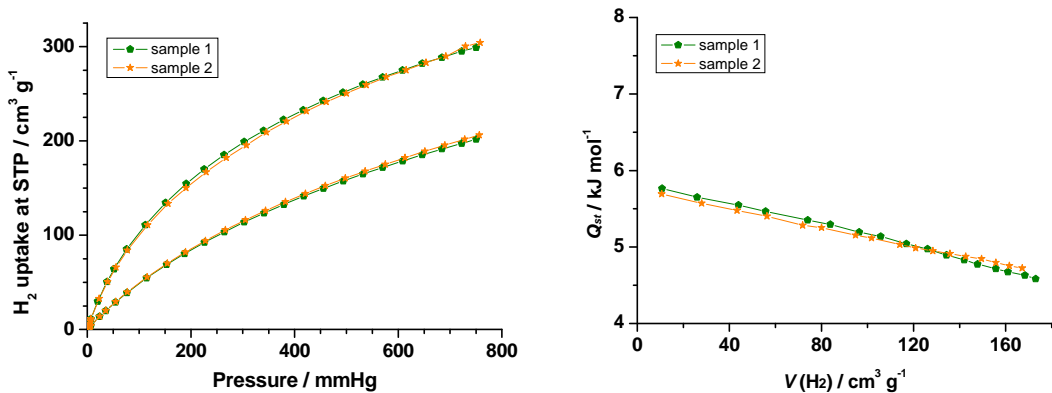


**Fig. S11** Two hydrogen sorption measurements for MOF **Cu-TPBTM** (the ligand is connected by three amide groups, *J. Am. Chem. Soc.*, 2011, **133**, 748.) (and corresponding  $Q_{\text{st}}$  calculated from the adsorption isotherms at 77 K and 78 K) by using two different samples.

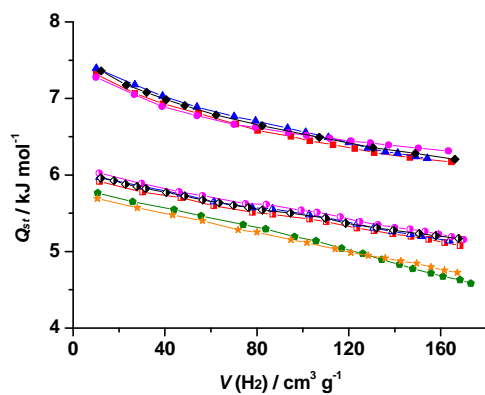


**Fig. S12** The comparison of  $Q_{\text{st}}$  for hydrogen adsorption of MOFs **Cu-ABTA**, **NTU-105** and **Cu-TPBTM**. As shown in **Fig. S9-12**, although there are no huge differences in the amount of hydrogen gas uptake among these three MOFs, however, some differences of the isosteric heat of adsorption ( $Q_{\text{st}}$ ) are presented. The results show that the  $Q_{\text{st}}$  of our reported MOF **Cu-ABTA** is higher than both of **NTU-105** and **Cu-TPBTM** instead of in between of them ( $\text{Cu-ABTA} > \text{NTU-105} > \text{Cu-TPBTM}$ ).

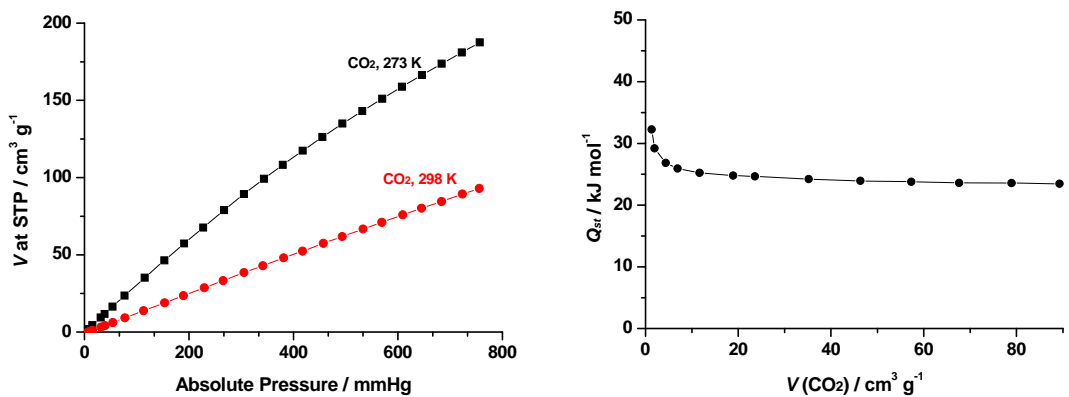


**Fig. S13** CO<sub>2</sub> adsorption isotherms (left) and isosteric heat of CO<sub>2</sub> absorption (right) for **NTU-105** calculated from the adsorption isotherms at 273 K and 298 K.

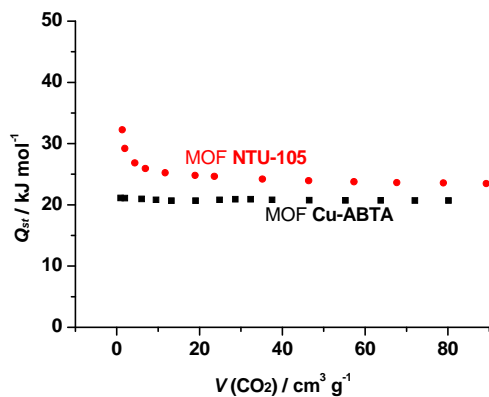
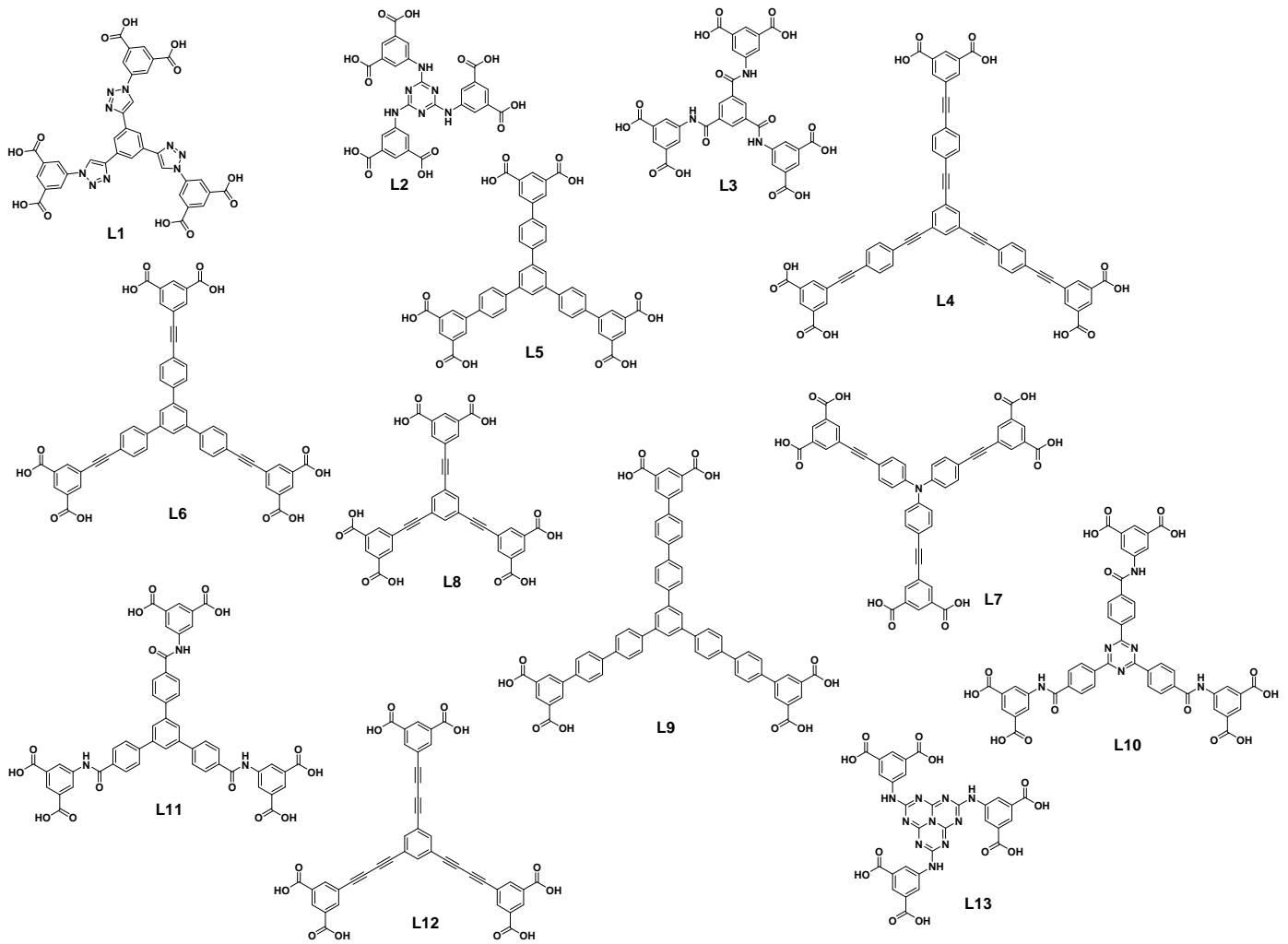


**Fig. S14** Comparison of isosteric heat for CO<sub>2</sub> adsorption of MOF **Cu-ABTA** and **NTU-105** under the same uptake amount.



**Scheme S2.** The chemical structure of reported  $C_3$ -symmetric ligands used in constructing *rht*-type MOFs.

**Table S1.** Summary of the porosities, and gas uptake capacities of various *rth*-type MOFs.

MOF [ligand]	$S_{\text{BET}}$ [ $\text{m}^2 \text{ g}^{-1}$ ] <sup>a</sup>	$V_{\text{pore}}$ [ $\text{cm}^3 \text{ g}^{-1}$ ] <sup>a</sup>	$\text{H}_2$ uptake [wt%] <sup>b</sup>	$\text{CO}_2$ uptake [wt%] <sup>c</sup>	ref.
<b>Cu-ABTA [H6-1]</b>	2840	1.19	2.75	30.1	This work
<b>NTU-105<sup>d</sup> [L1]</b>	3543	1.33	2.75	36.7	S1
<b>Cu-TDPAT<sup>e</sup> [L2]</b>	1938	0.93	2.65	44.5	S2
<b>Cu-TPBTM [L3]</b>	3160	1.27	—	42.6	S3
<b>NU-100<sup>f</sup> [L4]</b>	6143	2.82	1.82	12.3 <sup>g</sup>	S4
<b>NOTT-112 [L5]</b>	3800	1.62	2.3	—	S5
<b>PCN-68<sup>h</sup> [L6]</b>	5109	2.13	1.87	—	S6
<b>PCN-66 [L7]</b>	4000	1.63	1.79	—	S6,S7
<b>PCN-61 [L8]</b>	3000	1.36	2.25	—	S6,S7
<b>PCN-69<sup>i</sup> [L9]</b>	3989	2.17	1.72	—	S8
<b>Cu-TATB [L10]</b>	3360	1.91	—	17.3	S9
<b>Cu-BTB [L11]</b>	3288	1.77	—	17.2	S9
<b>NU-111 [L12]</b>	5000	2.38	2.1	—	S10
<b>rht-MOF-9 [L13]</b>	2420 <sup>j</sup>	1.01 <sup>j</sup>	2.72	25.3	S11

<sup>a</sup>calculated from  $\text{N}_2$  isotherms at 77 K; <sup>b</sup>at 77 K, 1 atm; <sup>c</sup>at 273 K, 1 atm; <sup>d</sup>also known as NOTT-122<sup>S12</sup> or NU-125<sup>S13</sup>; <sup>e</sup>also known as rth-MOF-7<sup>S14</sup>; <sup>f</sup>also known as PCN-610<sup>S6</sup>; <sup>g</sup>data at 298 K, 1 atm, due to the absence of the data at 273 K, 1 atm; <sup>h</sup>also known as NOTT-116<sup>S15</sup>; <sup>i</sup>also known as NOTT-119<sup>S16</sup>; <sup>j</sup>calculated from Ar isotherms at 87 K

## References:

- S1. X.-J. Wang, P.-Z. Li, Y. Chen, Q. Zhang, H. Zhang, X. X. Chan, R. Ganguly, Y. Li, J. Jiang and Y. Zhao, *Sci. Rep.*, 2013, **3**, 1149.
- S2. B. Li, Z. Zhang, Y. Li, K. Yao, Y. Zhu, Z. Deng, F. Yang, X. Zhou, G. Li, H. Wu, N. Nijem, Y. J. Chabal, Z. Lai, Y. Han, Z. Shi, S. Feng and J. Li, *Angew. Chem. Int. Ed.*, 2012, **51**, 1412.
- S3. B. Zheng, J. Bai, J. Duan, L. Wojtas and M. J. Zaworotko, *J. Am. Chem. Soc.*, 2011, **133**, 748.
- S4. O. K. Farha, A. Özgür Yazaydin, I. Eryazici, C. D. Malliakas, B. G. Hauser, M. G. Kanatzidis, S. T. Nguyen, R. Q. Snurr and J. T. Hupp, *Nat Chem*, 2010, **2**, 944.

- S5. Y. Yan, X. Lin, S. Yang, A. J. Blake, A. Dailly, N. R. Champness, P. Hubberstey and M. Schroder, *Chem. Commun.*, 2009, 1025.
- S6. D. Yuan, D. Zhao, D. Sun and H.-C. Zhou, *Angew. Chem. Int. Ed.*, 2010, **49**, 5357.
- S7. D. Zhao, D. Yuan, D. Sun and H.-C. Zhou, *J. Am. Chem. Soc.*, 2009, **131**, 9186.
- S8. D. Yuan, D. Zhao and H.-C. Zhou, *Inorg. Chem.*, 2011, **50**, 10528.
- S9. B. Zheng, Z. Yang, J. Bai, Y. Li and S. Li, *Chem. Commun.*, 2012, **48**, 7025.
- S10. O. K. Farha, C. E. Wilmer, I. Eryazici, B. G. Hauser, P. A. Parilla, K. O'Neill, A. A. Sarjeant, S. T. Nguyen, R. Q. Snurr and J. T. Hupp, *J. Am. Chem. Soc.*, 2012, **134**, 9860.
- S11. R. Luebke, Ł. J. Weseliński, Y. Belmabkhout, Z. Chen, Ł. Wojtas and M. Eddaoudi, *Cryst. Growth Des.*, 2014, **14**, 414.
- S12. Y. Yan, M. Suyetin, E. Bichoutskaia, A. J. Blake, D. R. Allan, S. A. Barnett and M. Schroder, *Chem. Sci.*, 2013, **4**, 1731.
- S13. C. E. Wilmer, O. K. Farha, T. Yildirim, I. Eryazici, V. Krungleviciute, A. A. Sarjeant, R. Q. Snurr and J. T. Hupp, *Energy Environ. Sci.*, 2013, **6**, 1158.
- S14. R. Luebke, J. F. Eubank, A. J. Cairns, Y. Belmabkhout, L. Wojtas and M. Eddaoudi, *Chem. Commun.*, 2012, **48**, 1455.
- S15. Y. Yan, I. Telepeni, S. Yang, X. Lin, W. Kockelmann, A. Dailly, A. J. Blake, W. Lewis, G. S. Walker, D. R. Allan, S. A. Barnett, N. R. Champness and M. Schröder, *J. Am. Chem. Soc.*, 2010, **132**, 4092.
- S16. Y. Yan, S. Yang, A. J. Blake, W. Lewis, E. Poirier, S. A. Barnett, N. R. Champness and M. Schroder, *Chem. Commun.*, 2011, **47**, 9995.